Passive radio-frequency identification ranging, a dense and weather-robust technique for landslide displacement monitoring

Mathieu Le Breton, Laurent Baillet, Éric Larose, Etienne Rey, Philippe Benech, Denis Jongmans, Fabrice Guyoton, Michel Jaboyedoff

Passive Radio-Frequency Identification Ranging, a Dense and Weather-Robust Technique for Landslide Displacement Monitoring

Mathieu Le Breton[a,b], Laurent Baillet[a], Eric Larose[a], Etienne Rey[a,b], Philippe Benech[c], Denis Jongmans[a], Fabrice Guyoton[b], Michel Jaboyedoff[d]

(a) Univ. Grenoble Alpes, ISTerre, CNRS, F-38000 Grenoble, France;
(b) Géolithe, 38920 Crolles, France;
(c) IMEP-LAHC, MINATEC, 38016 Grenoble, France;
(d) Institute of Geomatics and Risk Analysis, University of Lausanne, 1015 Lausanne, Switzerland;

Abstract— **Ground deformation monitoring at a local scale requires accuracy, along with dense spatio-temporal resolution. Radio-Frequency Identification (RFID) technology is proposed as an alternative to classical geodetic methods for monitoring displacements of a landslide. Passive RFID tags allow for a very dense resolution, both in time and space, at the scale of a 100-m-long surface. By deploying 19 passive RFID tags on a landslide for 5 months, this study validates the technique by comparison with laser total station and wire extensometer data. The accuracy of the RFID technique was 1 cm during normal weather and up to 8 cm during snow events. The results demonstrate that RFID tag tracking can monitor landslide displacements with multiple sensors at low cost, providing dense spatio-temporal data. This technique could potentially be used for other applications such as monitoring volcanic activity, buildings, unstable rocks or snow cover.**

Keywords — **Wireless sensor network, Slope stability, Real-time location tracking system, Early warning, Monitoring, Radio-Frequency Identification**

Highlight —

- Passive RFID is a new method to monitor surface displacements on a landslide.
- RFID works across vegetation, fog, rain and snowfall.
- This first prototype allows for a wireless monitoring at a range of 60 m.
- Displacement accuracy reaches 1 cm in general and 8 cm with a snow cover.
- Low-cost RFID tag network provides data with high spatio-temporal resolution.

Abbreviations

RFID: Radio-Frequency Identification

TD-Phase: Time-Domain Phase Difference of Arrival

FD-Phase: Frequency-Domain Phase Difference of Arrival

RSS: Received Signal Strength

1. INTRODUCTION

Ground deformations are monitored at different scales. On a scale of a few hundred meters, a landslide creates surface displacements that vary in both time and space. Motion monitoring to understand the landslide mechanism requires the best possible spatial and temporal resolution. However, obtaining a high spatial resolution is expensive at the scale of landslides, owing to either the station or the multiple measurement points. Large-zone monitoring techniques, such as ground-based radar interferometers, laser scanners, robotic total stations and fiber optics (Monserrat et al., 2014; Jaboyedoff et al., 2012; Iten et al., 2008) have a high station cost (30-100 k€), which restrict their use in standard applications. Similarly, more localized techniques such as GPS and extensometers have a cost per point (1-10 k€) that make them economically inefficient for a spatially-dense network of sensors (Gili et al., 2000; Angeli et al., 2000). The development of low-cost single-frequency GPS (Benoit et al., 2015) and radio-frequency transponders (Kenney et al., 2009; Intrieri et al., 2018a) reduced the cost to 100-1000 € per point, but each instrument still requires its own power source, which considerably increases the cost of the material, its installation and maintenance. Satellite Remote sensing techniques are economically efficient but their best current time resolution is 4-6 days (Intrieri et al., 2018b; Milillo et al., 2014; Lacroix et al., 2018). Similarly, ground-based optical correlation barely exceeds a 1-day resolution (Travelletti et al., 2012) because of low light at night and other luminance variations. Furthermore, some techniques are completely unusable in specific conditions: GPS signal may be blocked by steep slopes and high trees, optical techniques may be hindered by fog, rain, snow and vegetation, and extensometers may be obstructed by snow, ice or animals. In comparison, Radio-Frequency techniques continue to work in the presence of rain, fog, snow and vegetation, although environmental conditions may affect accuracy. Given these facts, Radio-Frequency Identification (RFID) (Heidrich et al., 2010) appears to be a viable alternative in terms of cost, spatio-temporal resolution and weather robustness.

Billions of passive targets, or tags, are produced by the RFID industry every year (Das, 2017) to identify goods remotely, leading to numerous research and business applications (Ngai et al., 2008; Tzeng et al., 2008). Tags typically comprise a passive microcircuit connected to an antenna. They communicate with a station that consists of a reader connected to another antenna. This communication relies on a continuous radio-frequency wave emitted by the station, this wave powers the tag, which then backscatters a modulated wave that encodes its own identification number, and the station reads this number (*EPC Gen2*, 2015). Passive tags and stations currently cost 0.01-20 € and 2-4 k€, respectively, and the reader can identify 30 to 800 tags per second (*EPC Gen2*, 2015; Klair et al., 2010). These

advantages have already been exploited in RFID applications in earth-science research, such as to sense soil moisture levels or vibrations (Pichorim et al., 2018; Jayawardana et al., 2016), measure crack openings (Cazeca et al., 2013; Caizzone and DiGiampaolo, 2015), or trace alluvial and coastal sediment (Lamarre et al., 2005; M. H. Nichols, 2004). However, continuous displacement monitoring with RFID remains untested outdoors.

Several methods have been developed to locate passive tags (Miesen et al., 2011). These methods usually estimate the 1D range or displacement between a tag and a station antenna, and optionally locate the tag in 2D or 3D using multiple station antennas. These ranging techniques can use the Received Signal Strength (RSS) (Griffin and Durgin, 2009; Ni et al., 2003), the Phase Difference of Arrival (Vossiek and Gulden, 2008; Nikitin et al., 2010) or more recently the Time of Flight (ToF) (Arnitz et al., 2010; Arthaber et al., 2015). Currently, phase-based methods are compatible with commercial readers and offer the best accuracy. Several studies used the phase to localize tags with an accuracy of one centimeter or less. However, these experiments were of short duration (<1 h), over a short range (<10 m) and were performed indoors. When these techniques are used outdoors, environmental fluctuations could affect their accuracy. A previous study showed that moisture and temperature variations could create a phase drift of up to 20 cm over a year (Le Breton et al., 2017). Corrections were proposed, which reduced that drift to less than 2 cm per year, with a reversible error of 7 mm induced by rain. However, the short tag-station distance (6 m) limited the effect of multipath propagation in that study. The effect of multipath propagation may be increased at long range and outdoors and passive RFID has never yet been studied in these conditions.

Hectometer-range outdoor radio-frequency ranging has nevertheless been assessed on landslides using active transponders. The ranging techniques were based either on RSS, ToF or Phase, with displacement accuracies of 100, 5 and 1 cm, respectively (Lucianaz et al., 2015; Intrieri et al., 2018a; Kenney et al., 2009). Since these techniques use the same physical principles as passive techniques, phase-based RFID ranging is also expected to have a displacement accuracy of 1 cm outdoors. As to the maximal range attainable, manufacturers claim ranges of up to 60 m for passive tags (Confidex, 2014); this range may be sufficient for the goals of this study.

The previous studies then suggest that a dense network of passive RFID tags could be deployed on hectometer-scale landslides at low cost, to monitor 1D radial displacements with an accuracy of 1-2 cm in a variety of meteorological conditions. To test the performance of RFID, for five months, we monitored the displacements of 19 tags placed 5 m apart on a medium-sized landslide (Pont-Bourquin, Switzerland) and compared the results to those obtained with total station and extensometer data. We provide an example application that benefit from the RFID technique, studying the

relation between the rainfall and the velocity of this landslide, and finally discuss the advantages and limitations of RFID displacement monitoring.

2. MATERIAL AND METHODS

2.1. Experimental site: Pont-Bourquin landslide

The Pont-Bourquin landslide lies in the Swiss Pre-Alps, 50 km southeast of Lausanne (Fig. 1.a). The landslide crosses a complex geological zone composed of Triassic to Jurassic sediments, including gypsum, cargneule, shale siltstones and black shales, separated by tectonic thrusts (Badoux et al., 1990). Quaternary moraines partially cover the slope. The landslide material thus mixes all these sediments, with a dominant proportion of clay produced by degradation of black shale.

The landslide is about 240 m long, 30 m large (Fig. 1.b) and 10 m deep (Jaboyedoff et al., 2009). Its average slope is around 25° facing south. The total landslide volume is approximately 40 000 m^3, which includes an active part of around 11 000 m^3. The landslide mostly moves translationally, with a slight rotation at its top. Orthophotos from 1995, 1997 and 2004 revealed continuous degradation due to slope movements and erosion in the landslide area. In 2006, a scarp of 0.8 m was observed at the top of the landslide. On 5 July 2007 a sudden earthflow of around 3 000 to 6 000 m^3 occurred after 95 mm of rain fell over a 3-day period (Jaboyedoff et al., 2009). In subsequent years, the landslide permanently moved by a few meters per year, before suddenly accelerating its descent in summer 2010 leading to a mudflow of a few thousand cubic meters that blocked the road downslope on 19 August 2010 (Mainsant et al., 2012). Due to its continuous activity, this landslide appears to be a good candidate to test the RFID technique over several months.

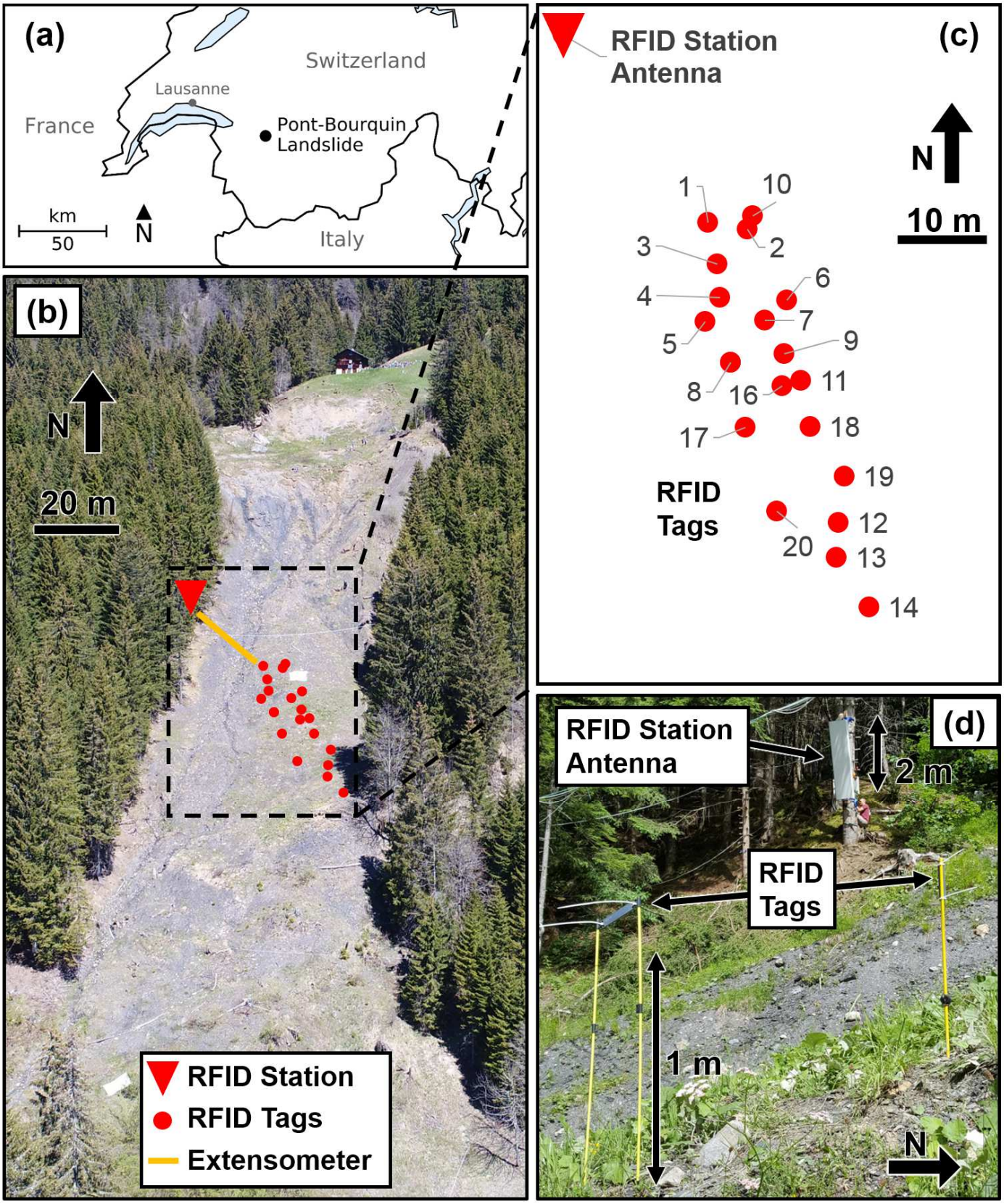

Fig. 1. (a) Pont-Bourquin landslide location in Switzerland (46.3518N, 7.1780E), (b) General aerial view of the Pont-Bourquin landslide, (c) zoom on the zone where instruments were placed (black rectangle in b), showing the tags and the RFID station, and (d) photograph showing tags No. 10 and No.°2 installed on the landslide, and the station which is placed on a stable zone.

2.2. **Monitoring instruments**

On 3 July 2017, the Pont-Bourquin landslide was equipped with the RFID material proposed previously by Le Breton et al., (2017) that reduces the influence of water and temperature on the phase. The acquisition system was composed of a stable station, 19 moving tags, and a remote server. The station was installed on a tree 3 m above the landslide's surface and comprised a reader, an antenna and a computer (SR420 from Impinj and model 80010643 from Kathrein). It typically required 20 W power under continuous operations, which was provided through the Swiss power grid. The station collected about 20 Mo of data per day by measuring the phase difference of arrival and the temperature on 30 tags per second, using a randomized tag interrogation order (*EPC Gen2*, 2015). This corresponds to the slowest and most accurate mode of interrogation available on the reader (Dense M8). The reader was chosen because it provided the most precise phase measurements and the best sensitivity (and therefore reading range) and is well adapted for use with slow-moving objects. The phase-shift measured was limited within the range $[0, \pi]$ (Miesen et al., 2013b). The tags were installed on 0.9-m-high fiber-glass stakes that were planted in the unstable slope (Fig. 1.d). The tags were elevated above the ground because preliminary tests indicated that placing tags near the ground considerably reduced the RSS, down to -30 dB at ground-level. These tags were placed within the zone covered by the RFID antenna, which measured approximately 40x10 m (Fig. 1.b-c), and remained within the line-of-sight of the station antenna during the experiment. The tags (Survivor B, from Confidex) comprised a solid plastic casing (155×26×14 mm) protecting a patch antenna (+0.6 dBi effective gain and ±65 °E / ±80 °H beam-width at 3 dB) and a battery-assisted microcircuit (EM4325 from EM Microelectronic). While assisted by a tiny button cell to boost their reading range, the tags remain passive: they backscatter the interrogator carrier wave the without amplification, and the exactly same technique work with batteryless tag. In term of lifetime, the tag's battery may last 5 to 20 years under continuous interrogation, given the cell of 290 mAh and the typical micro-circuit current of 1.7-6 μA (*EM 4325 Spec.*, 2015). This lifetime may be shortened by battery aging and by the extra temperature measurements, but still last several years according to the tag manufacturer (Confidex, 2014) and to our own experience.

To validate the RFID measurements, we installed a wire extensometer (ASM WS17KT) between a metallic stake (0.5-m-high, 0.7-m-deep and 1 meter away from tag No. 10) and the bottom of the station antenna. We extended the original 2.5-meter Invar wire with a 20-meter Kevlar wire. An acquisition card (Campbell CR1000) measured the length of the extensometer wire every minute, representing a radial displacement along the line of sight of the antenna. During processing, the displacement from both the extensometer and the RFID was averaged every hour.

We also measured the 3D coordinates of the tags and base station on 27 July and 6 October using two manual total station surveys (Leica TCR805), to compute the 1D tag-station radial distance and its difference between the two surveys. The positions of the extensometer and tags No. 10 and 11 were measured using a fixed reflector, with an accuracy of ± 5 mm. For the other tags, the manual positioning of the prism resulted in lower accuracy, estimated at ± 2 cm. Hence, the accuracy of the relative displacement between two total station surveys was ± 1 cm for tags No. 10 and 11, and ± 4 cm for the other tags.

Finally, we used data provided by MétéoSuisse related to fresh snow height and total snow height (measured daily at 6 am at Diablerets village, 1 km away), precipitations, humidity, air temperature (every 10 minutes at Col des Mosses, 6 km away) and pressure (every 10 minutes at Les Diablerets).

2.3. **RFID ranging methods**

This study first compares two absolute ranging techniques (FD-Phase and RSS) with a relative displacement technique (TD-Phase). Firstly, the relative radial displacement of a backscattering tag can be computed in free space using the Time-Domain Phase Difference of Arrival technique (TD-Phase) (Nikitin et al., 2010), as presented in Fig. 2, with

$$\delta r = -\frac{v}{4\pi f}\delta\varphi_{air} \qquad (1)$$

where

φ_{air} phase-shift resulting from propagation through air;

r distance between the station and the tag;

v RF wave velocity in the medium ($\approx 2.998 \cdot 10^8$ m/s);

f carrier frequency (= 865.7, 866.3, 866.9 or 867.5 MHz as defined by *ETSI-EN 302-208* (2016)).

In this application, the reader measures the phase difference of arrival between [0, π] modulo π. Using equation (1), this phase interval is equivalent to a distance of 8.6 cm, or ± 4.3 cm. Larger displacements are ambiguous to measure directly and require phase unwrapping, by adding or subtracting 8.6 cm when the difference between two consecutive measurements exceeds ± 4.3 cm.

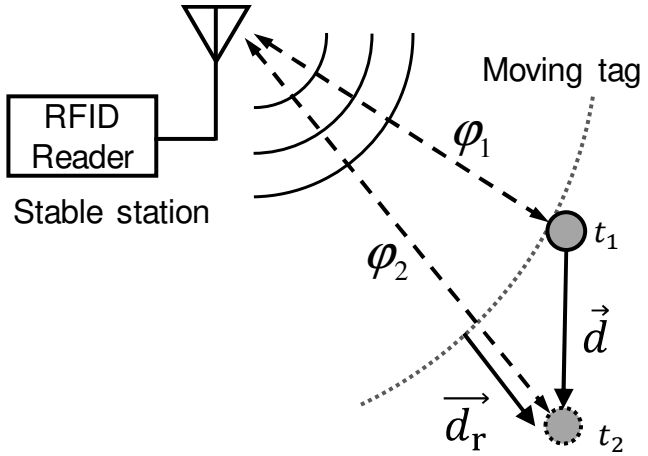

Fig. 2. Schematic representation of how tag displacement is tracked by a static station. The phase variation measures the radial displacement $\mathbf{d_r}$ between two acquisitions.

Secondly, the absolute distance *r* can be computed by measuring the phase at different frequencies, based on the Frequency-Domain Phase Difference of Arrival (FD-Phase) technique (Nikitin et al., 2010) :

$$r = \frac{\delta\varphi_{air}}{\delta f}\frac{v}{4\pi} - r_0 \qquad (2)$$

where

$\delta\varphi_{air}$ phase difference resulting from the change in carrier frequency;

δf difference in frequency between two carrier frequencies (0.6 MHz);

r_0 offset due to wave propagation in cables and instruments (11 m).

The resulting distance r was computed for each of the three available frequency intervals and averaged. As long as tags are placed at less than 125 m (minus r_0) away from the station antenna, this technique provides an absolute distance without ambiguity. The unique offset r_0 used on all the tags was initially calibrated from tag No. 10 as 11 m, for which the range to the station (22 m) was measured using the total station on July 27.

Thirdly, the absolute distance *r* can be estimated from the attenuation of the received power (RSS) over a two-ways propagation (Griffin and Durgin, 2009). As the RSS depends on the station and tag gain, their relative orientation, and the environmental conditions (Dobkin and Weigand, 2005), it requires calibration based on reference tags placed at a known distance (Ni et al., 2003). We computed one virtual reference tag, from the average RSS and tacheometric distances of all the tags over the first month. The absolute range r_i of tag i can then be estimated by comparing its received power *P* to that of the reference tag, using:

$$r_i \approx r_{ref} \sqrt[4]{P_{ref} / P_i} \quad (3)$$

These three absolute and relative ranging techniques are compared in section 3.1. The remainder of the article then focuses solely on the TD-Phase relative displacement measurements.

3. RESULTS

3.1. Performance of the different RFID ranging techniques

The absolute distance covered by each tag was computed from the Frequency-Domain Phase (using (2)) and the RSS (using (3)) and compared to the total station laser measurements (Fig. 3). The range values were computed every hour and averaged over a 5-month period. The vertical bars represent the drift over this whole period, based on the 90% confidence interval. The curve shows that the RSS-based ranging measurements follow an increasing trend with distance from the station, but that some strong outliers are found, as are large drifts of up to ±15 m. These datapoints were due to the strong impact of uncontrolled parameters: environmental variations, antenna orientation and ground reflection interference. Therefore, the method cannot be considered reliable. In contrast, the distances obtained with the FD-Phase method gave a good fit with the distances measured with the total station, with a maximum drift of ± 2 m. This level of error is still too high for our monitoring purposes, but it can be reduced by using relative displacement techniques.

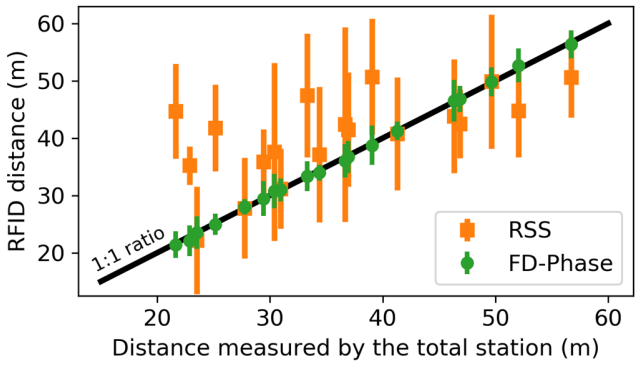

Fig. 3. Comparison of the radial distances between the tags and the station antenna estimated by RFID ranging techniques (RSS and FD-Phase) with this same distance measured by a manual total station, for the 19 tags deployed. The vertical bars represent the amplitude of the drift over the 5-month period, and the width of the 1:1 ratio line represents the true displacement over 5 months. The centimeter-scale total station error is negligible, and was therefore not represented.

The relative displacements of tag No. 10 over time, computed from variations in FD-Phase, RSS, and TD-Phase are compared in Fig. 4, along with the total station measurements. The FD-Phase and RSS show significant variations over

time, which can be up to 4 m. In contrast, the TD-Phase measurement appears much more stable and accurate than the RSS and FD-Phase ranging techniques when monitoring relative displacements. Indeed, the relative displacement is more sensitive to phase or frequency errors in equation (2) compared when applying (1). The TD-Phase results appear coherent with those provided by the total station, and are validated in more detail in the next section by comparison with standard ranging techniques.

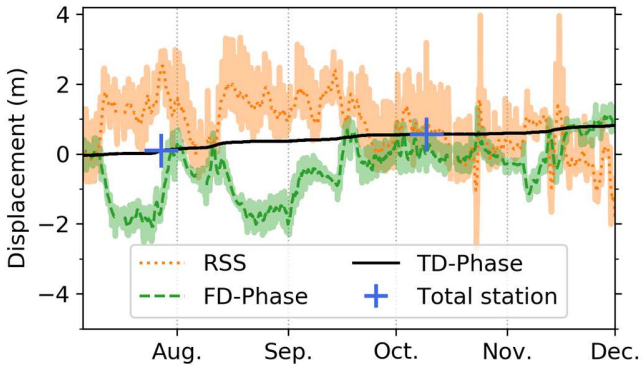

Fig. 4. Relative radial displacement between RFID tag No. 10 and the station antenna over a 5-month period, using the Received Signal Strength (RSS), the Frequency-Domain Phase Difference of Arrival (FD-Phase) and the Time-Domain Phase Difference of Arrival (TD-Phase) techniques, compared to the radial displacement computed from total station measurements. The darker lines for RSS and FD-Phase represent a 24-h moving averaged.

3.2. **Validation of the TD-Phase RFID technique**

The TD-Phase displacements are compared with the automatic wire extensometer measurements over 4 months and with the two manual total station surveys (Fig. 5). The tag studied (No. 10) was installed next to the extensometer stake. The RFID curve appears to match the extensometer data although a slight discrepancy appeared in September, which progressively increased to around 5 cm difference at the end of the observation period. The total station data showed that this discrepancy was caused by a true differential displacement between the tag and the extensometer, which were installed on separate stakes. Another difference was that the wire extensometer curve was noisier and exhibited several strong spikes from mid-October, which appear to be linked to snowfall (Fig. 5b): snow accumulation bent the wire down, pulling the cable along by several decimeters, such as on October 20. This extra length remained until snowmelt or until the cable was manually dug out from under the snow. RFID tracking thus provided better continuity and accuracy over time than the wire extensometer. In particular, the error due to snowfall was smaller and restricted in time to the precipitation episode.

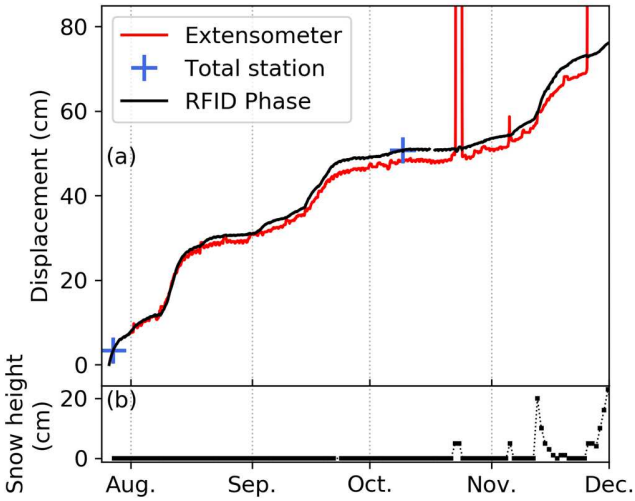

Fig. 5. (a) Cumulative radial displacement measured over 4 months on the Pont-Bourquin landslide, using a wire extensometer, the phase of RFID tag No. 10, and a manual laser total station. (b) Total snow height. The snow considerably perturb the wire extensometer measurements.

The landslide velocity computed from the RFID (tag No. 10) and the extensometer data are shown in Fig. 6.a-b. Each velocity was derived from the displacement, after the application of a low-pass filter (1-day moving average) to reduce the cyclic daily drift. The RFID velocity curve appears more stable than the extensometer velocity curve. Indeed, rain- and snow-fall (Fig. 6.c-d) created numerous positive and negative peaks on the extensometer velocity curve. That resulted from the additional water or snow weight that temporarily increasesd curvature in the wire. In comparison, the RFID velocity curve shows almost no perturbation due to rain and the artifact caused by snow was much smaller (± 1 cm/day).

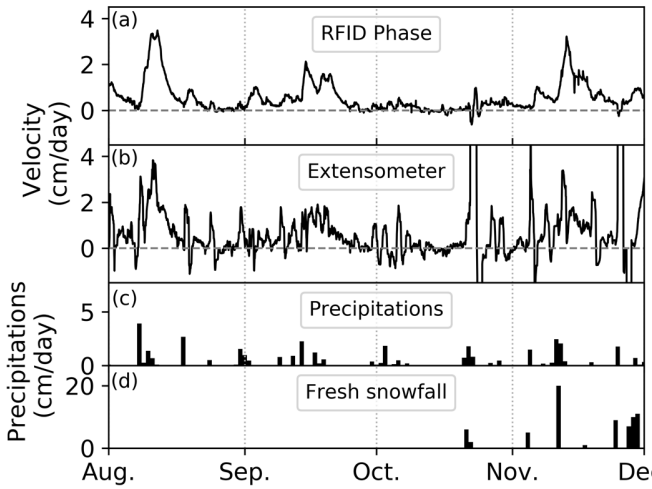

Fig. 6. Comparison of radial velocities between (a) RFID tag n°10 and (b) extensometer after filterAing for daily variations. (c) Rainfall and (d) fresh snowfall are also shown.

225

226 To illustrate its capacity to monitor multiple tags, the RFID cumulative displacement (Fig. 7) and the velocity for all
227 tags (Fig. 8) were plotted over the five-month period. The cumulated displacement ranged between 0.69 and 0.94 m
228 (extremes measured for tags No. 12 and No. 7, respectively). The shape of the displacement curves was similar on all
229 tags, suggesting that the zone studied moved in the same way during the observation period. Locally, some
230 displacement measurements may have been affected by a rotational motion of the stick, observed from pictures as ± 7°
231 during the 5-month period. Such motion of the stick would cause a ± 12 cm displacement of the tags, which is the same
232 magnitude as the motion discrepancy between tags. However, the similarity between all the curves indicates that this
233 effect was progressive and smaller than the ground displacement. The velocity for all tags is shown in Fig. 8. The
234 curves were ordered according to a noise indicator, computed as the standard deviation of the detrended total
235 displacement, with additional weight for the heavy rainfall recorded between September 30 and October 3. As a result
236 of this ordering, the more accurate curves are placed at the bottom of the figure. Each tag measured the true
237 displacement of the landslide surface, added to an instrumental artifact due to rain. The amplitude of this rain artifact
238 was quite distinct from one tag to another (e.g. between September 30 and October 3) and results in heterogeneous
239 accuracies.

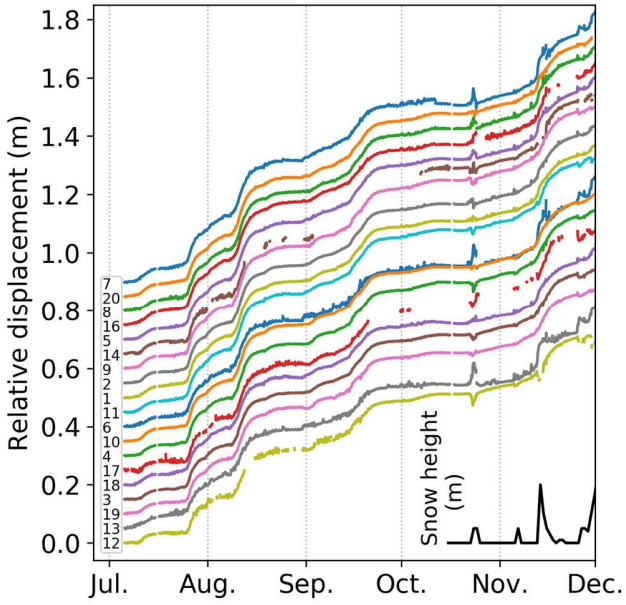

Fig. 7. Radial displacement curves for all tags over 5 months. The curves are ordered based on their cumulative displacement using a vertical offset to facilitate vizualization. The inset indicates the snow height.

240

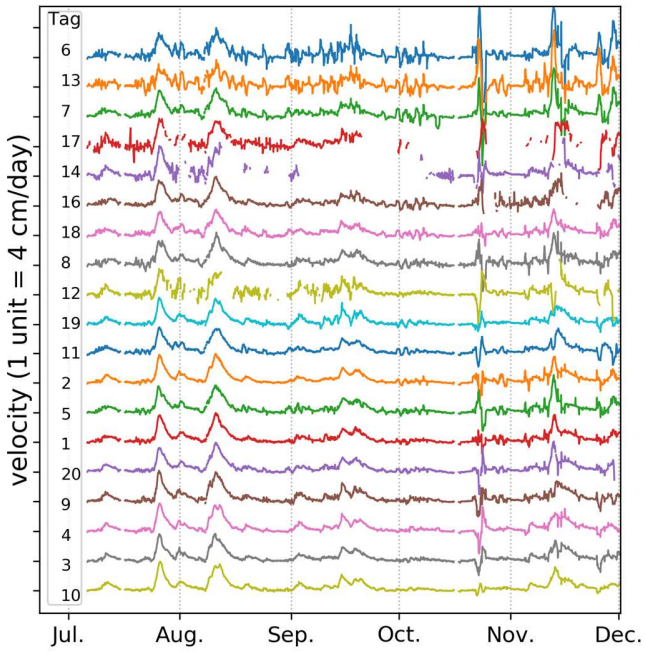

Fig. 8. Radial velocity curves for all tags, ranked by decreasing noise levels from top to bottom.

241

242 3.3. **Precision, trueness and robustness of the TD-Phase technique**

243 To determine the validity limits of the RFID TD-Phase technique, we tried to quantify its precision, trueness and

244 robustness from the five-month experiment. The accuracy indicators are computed from the experimental data and
245 summarized in Table I for precision and trueness, and Table II for robustness. The accuracy is then given by the
246 combination of the precision and the trueness.

247 *Precision*

248 The precision is given by the random measurement error estimated from the phase standard deviation over one
249 minute, a timespan that is short enough to allow systematic error due to meteorological variations to be neglected. This
250 random measurement error was then plotted against the RSS (Fig. 9). The random measurement error appears to obey
251 the relation $\sigma_r = \alpha / \sqrt{P}$ (4) with the received power P, using an interrogator-dependent coefficient
252 $\alpha=9.5\cdot10^{-9}$ m·W$^{1/2}$. The curve obtained is coherent to the phase signal-to-noise ratio observed by Vossiek and Gulden
253 (2008) that depends on the distance. On a single measurement, our random measurement error 3σ represent 0.1 to
254 1.3 cm (Table I), for a received power of $10^{-8.3}$ to 10^{-6} mW. This random error can be statistically decreased to
255 0.01-0.17 cm by averaging 60 measurements over one minute, it thus becomes negligible compared to the systematic
256 measurement error presented below.

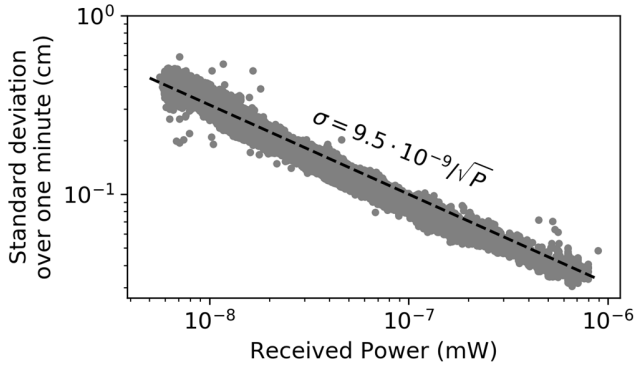

Fig. 9. Random measurement error represented as the standard deviation σ_r computed every minute for each tag, plotted against the received power *P*, on a logarithmic scale. The curve shows a clear linear relation between $\sqrt{P}$ and σ_r.

257

258

TABLE I
TRUENESS AND PRECISION OF THE RIFD TECHNIQUE

	Number of samples	Deviation 99.7% confidence[(a)] (cm)
Radial Trueness		
Versus total station – all tags	19	5.3 (centered on 0.6)
tags No.10&11 only[(b)]	2	1.0 (centered on -0.05)
Versus 24h-smoothed data	60 000	1.1
During the first snowfall[(c)]	19	8.0
Radial Precision		
of a single reading[(d)]	$7x10^7$	0.1-1.3
over one minute	$4x10^6$	0.01-0.17

(a) The 99.7% confidence interval was computed from the Student law when there were less than 2000 samples and directly from the equivalent quantile when there were more than 60 000 samples. The distributions were verified to ensure they were close to a normal law.
(b) Tacheometric surveys were more accurate for tags No. 10 & 11, and their fixation on a single sealed stick was more stable.
(c) The first snow fell between October 21, 18:00 and October 24, midnight, when tags showed a strong measurement bias. This was the worst bias accuracy observed.
(d) The precision of a single reading was linear with the signal amplitude, and followed the law $\sigma_\varphi = \alpha / \sqrt{P}$, with $\alpha = 1 \cdot 10^{-8}$ m·W$^{1/2}$

Trueness

The trueness is given by the systematic measurement error, estimated as the bias between the true value and the mean of the measured values. It includes the drift over time (days to months) and the inaccuracy over spatial displacements. Table I shows the displacement accuracy computed from the difference between the RFID technique and the total station surveys used as reference measurements. The average displacement measured for all tags by both methods differed by only 6 mm. Hence, the displacement of all the RFID tags appears coherent and, on average, unbiased compared to the total station data. However, the results are spread statistically over ± 53 mm within the 99.7% confidence interval. This spread mostly corresponds to the error when placing the optical reflector on the tags for the manual total station surveys: we have estimated this survey error to be ± 40 mm for most of the tags. The tags No. 10 and 11 were installed on a single stick, which improved the estimated survey error to ± 10 mm. For these two tags, the difference compared to the RFID measurements remained below 0.5 mm, which, given the small number of samples, corresponds to a potential error of ± 10 mm within the 99.7% confidence interval. In fact, the reference technique – manual total station – appears as or less accurate than the RFID method that is tested, and thus another method is required to assess the trueness.

The systematic measurement error with RFID is mostly due to environmental variations such as temperature, humidity and moisture, which vary over the course of a day (Le Breton et al., 2017). To estimate this systematic measurement error, we computed the RFID residual displacement amplitude after removing the

1-day-moving-averaged trend. These calculations showed a daily drift of less than 11 mm 99.7% of the time. Finally, the worst errors were observed during the first snowfall (see photo in Fig. 11), which triggered reversible displacement peaks of up to 79 mm, either positive or negative.

Hence, we estimate the trueness of this RFID method to be approximately 1 cm on a real landslide application under mixed meteorological conditions (dry, rain, snow), except for the first snowfall which appeared to limit the trueness to about 8 cm. Because the systematic error is much larger than the random one after averaging, we consider that this trueness also represent the total accuracy.

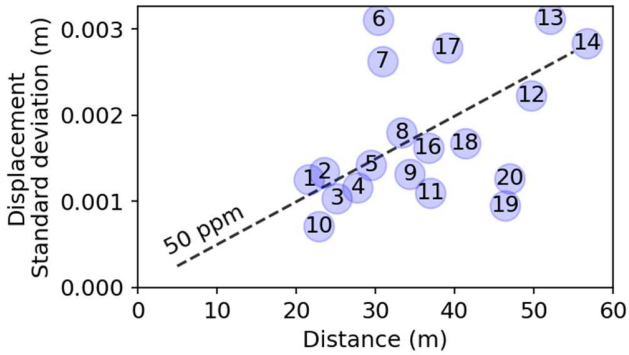

Fig. 10. Standard deviation of the 1-hour resampled RFID displacement after trend removal, plotted against the tag radial distance, for each tag. The deviation tends to increase with distance, at a rate of about 50 parts per million.

The measurement error could be partly related to the tag-station distance. To verify this relation, the standard deviation was plotted against the distance (Fig. 10). This analysis shows that the systematic measurement error tends to increase the measured distance by about 50 parts per millions (ppm), or 150 ppm for 3σ. This trend could be related to the following distance-dependent effects: Firstly, the atmospheric conditions influence on wave velocity (Gage and Balsley, 1980) could induce a +/- 3.4 ppm standard deviation (after detrending), computed from the meteorological data. Secondly, the interrogator frequency instability could result in variations of +/- 10 ppm, in line with the regulations (*EPC Gen2*, 2015). Thirdly, the amount of vegetation crossed by ground-reflected waves will increase with the distance, and its properties (such as height or water content) may vary over time and affect the overall signal (Kim et al., 2012). Fourthly, the greater the distance between the tag and the station, the more opportunities for multipathing due to the topography, and therefore potentially the greater the systematic error due to multipathing.

Fig. 11. Photo illustrating the two main sources of inacurracies in this experiment the snow (particularly the first snowfall) and the angle of the tag supports, which created a reversible error of 4.9 cm (3σ) at the end of October and a slow drift roughly estimated at up to 5 cm per month, respectively. Apart from those two specific problems, the accuracy remained below 1.1 cm (3σ).

296

297 *Robustness*

298 The robustness can be defined as the ratio between the total monitoring time and the time when the RFID is
299 operational. This is an important indicator for operational monitoring. Failure to identify the tags disqualifies the
300 monitoring. Table II shows the availability ratio for each tag over the observation period; 14 out of 19 tags were
301 available 97.5% of the time. The 2.5% unavailability was the result of software and network errors on the station. The
302 availability of the other tags ranged from 96 to 55%. Snowfall clearly affected communication with tags No. 16 and 20.
303 For other tags, the RSS was close to the limit of interrogator sensitivity (-83 dBm) due to either their distance (No. 12
304 and No. 14) or their angle relative to the station's antenna (No. 17). Signal strength may have been reduced by
305 destructive multipath interference at a specific tag position, and increased again once the tag moved forward.

TABLE II
OVERALL MEASUREMENT AVAILABILITY

Tags	Availability[(a)]	Major cause of problems
74% of the tags	97-98%	Software/network errors
No.20	96%	Snowfall of 29 Nov.
No.16	87%	Snowfall
No.12	82%	Large distance + interferences
No.17	55%	Station antenna directivity + interferences
No.14	55%	Largest distance

(a) Availability was computed after resampling the data every hour

306

307 **4. SAMPLE APPLICATIONS: COUPLING BETWEEN DISPLACEMENT AND PRECIPITATIONS.**

308 This example demonstrates how all-weather, dense displacement measurements can help to better characterize
309 landslide behavior, by analyzing the relation between rainfall and velocity data.

4.1. **Computation of the rainfall-related impulse response**

Precipitations often control the displacements of reactivated landslides by the intermediate of groundwater infiltration (Corominas et al., 2005) and subsequent changes of rheology, we will examine this effect in this section. The velocity/precipitation curves shown in Fig. 6 suggest that Pont-Bourquin landslide reacts directly to precipitation. The Impulse Response (IR) of velocity to rainfall on a reactivated landslide (Belle et al., 2014; Bernardie et al., 2015) can provide empirical insights into the behavior of this type of landslide, as long as no dramatic rupture occurs

The shape of the IR was first estimated by cross-correlating the precipitations with the velocity of the tag No. 10 between 3 July and 1 October. The cross-correlation on Fig. 12 shows a peak velocity approximately 1.2 days after the rainfall followed by a decrease in velocity until day 5-6, as already observed on this site (Bièvre et al., 2018). However, the correlation technique results in a poorly defined IR, producing an unrealistic reaction of the landslide's velocity before the start of the precipitations.

To improve the resolution, the IR was deconvoluted using the linear Lasso regression (Tibshirani, 1996) implemented in the scikit-learn library (Pedregosa et al., 2011), to minimize the following cost function:

$$J = 0.5\left\|Y - X\beta\right\|_2^2 + \lambda\left\|\beta\right\|_1 \qquad (5)$$

where

β IR vector; each β_n corresponds to the response after $n = 0,1 \ldots N$ hours of lag, N=120 here;

Y velocity vector; each Y_m corresponds to the velocity during the $m = 0,1 \ldots M$ hours of the observation period, 3 months here;

X precipitation matrix, where each $X_{m,n}$corresponds to the precipitations measured $m - n$ hours after the start of the observation period;

λ regularization parameter, to avoid over-fitting and causing the β parameters to tend toward zero. A value of 0.04 was chosen based on preliminary cross-validation tests.

This process provided a slight under-estimation of the IR amplitude because the regularization factor causes the values of β to tend toward zero. For this reason, the IR was later corrected with a factor (1.7 in this study) to equalize the measured and modeled velocities (the modeled velocity is presented in the next section).

4.2. **Impulse response and velocity model**

The IR (Fig. 12) was estimated using data collected from tag No. 10 between 3 July and 1 October (before snow).

337 This response suggests that the landslide remained stable for five hours after rainfall, then accelerated rapidly until it
338 reached a peak velocity after 18-24 h, and finally returned to a null velocity after 4.5 days. This pattern might
339 correspond to an initial infiltration in the superficial layers while the landslide remains stable, followed by a pore
340 pressure increase and then decrease in the aquifer as the landslide accelerates then decelerates. The lag before the
341 velocity peak was coherent with the 20-hour delay prior to elevation of the water table, measured previously in this
342 zone (Brönnimann, 2011). In addition, the shape of the IR curve is similar to a typical water infiltration process
343 (Iverson, 2000).

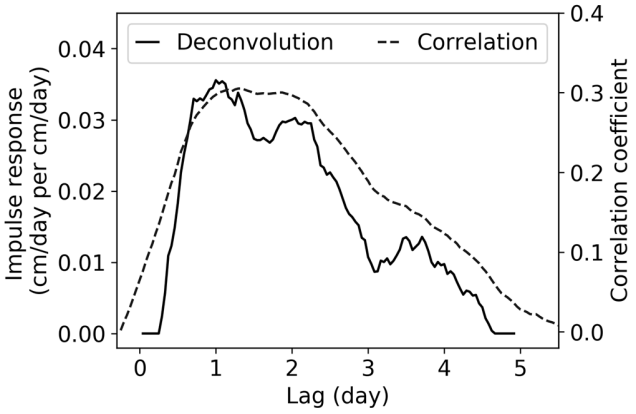

Fig. 12. Impulse response of landslide velocity (cm/day) following precipitation (cm/day) estimated by cross-correlation and Lasso regression deconvolution on rainfall and displacement data from tag No.10 over the 5-month period.

344

345 As the landslide may behave differently depending on the point measured or instrument used, the IR for all tags and
346 the extensometer are shown in Fig. 13. For the RFID, the darkest curves correspond to less noisy data, based on a noise
347 indicator, which represents both the instrumental sensitivity to rain and the random noise (see section 3.2). All the tags
348 showed a similar IR, and the discrepancy observed mostly depended on the instrumental bias due to rain, which is
349 added to the landslide IR. In contrast, the IR computed from the extensometer data was very different for the first two
350 days, showing a maximum peak almost during the rain event, before decreasing a null value and finally showing
351 similar results as from RFID after the second day. This pattern of landslide behavior is unrealistic, and can be explained
352 by a domination of the instrumental response, affected by the rain. This domination consequently prevents the
353 extraction of synthetic information from the landslide, such as the IR peak velocity, the lag time before it is reached and
354 the deceleration rate.

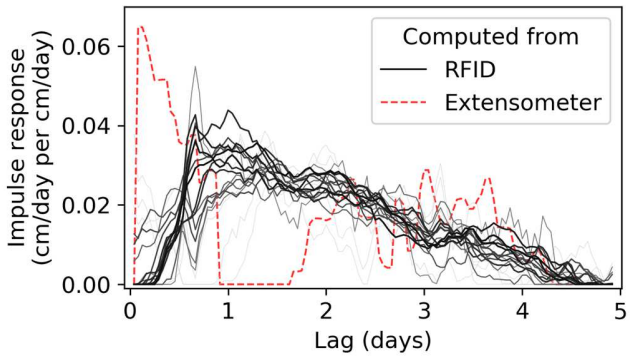

Fig. 13. Impulse response of the landslide velocity (cm/day) to precipitation (cm/day) deconvoluted using a Lasso regression on the velocity measured by all the RFID tags and the extensometer. For the RFID, darker lines represent more accurate tags, presenting lower noise and a lower sensitivity to rain.

Convolution of the IR with the precipitations can be used to compute a rain-based velocity model (Belle et al., 2014; Bernardie et al., 2015). Fig. 14 shows this velocity model superimposed on the velocity measured. Visually, the model appears coherent with the measurements, except on October 23, when the first snowfall was recorded. This coherence is confirmed by the cross-correlation of both curves that reach their maximum coefficient of 0.76 after a zero-hour lag.

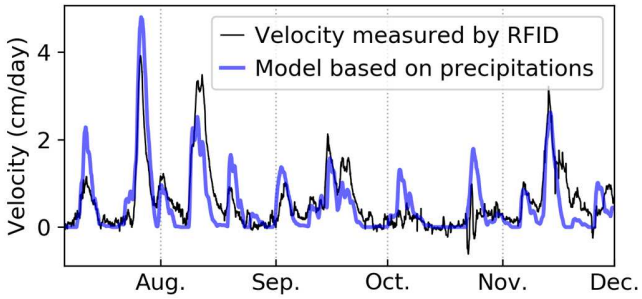

Fig. 14. Landslide radial velocity measured on tag No.10 compared to the model obtained by convoluting the precipitation with the deconvoluted impulse response. The time-series starts in July, one month earlier than that shown in Fig. 6.

4.3. **Advantages of RFID data for the IR approach**

This empiric IR method produced a relatively good fit between the measured and modeled velocity, for which the advantages and limitations are discussed in (Belle et al., 2014; Capparelli and Versace, 2011). This example emphasizes the potential of dense and continuous in situ displacement data, as provided by the RFID technique. As the IR is likely to be heterogeneous across a landslide area, placing multiple sensors enables the delimitation of these zones and provides a redundancy benefit. In this example, continuous data unaffected by rain and fog, with an hourly sampling time and sub-centimetric accuracy was also required to compute the IR. Observation of how this response

368 changes over time could provide an additional risk indicator, and would require continuous time series covering
369 several months or years. RFID is once again compatible with these measurements because of the low investment
370 necessary and the reduced maintenance cost. This application therefore highlights several advantages of the RFID
371 technique, which will be more fully discussed in the next section

372 ## 5. ADVANTAGES AND LIMITATIONS

373 The assessment of RFID relative ranging on a landslide has shed light on its advantages and limitations, which will
374 help guide future monitoring applications.

375 The major advantage identified in this study is that RFID works at night and under all meteorological conditions.
376 Indeed, radio-frequency waves are known to propagate in rain, fog, snow (Monserrat et al., 2014) and vegetation
377 (Intrieri et al., 2018a). Passive RFID in particular has been tested without line-of-sight (Wang and Katabi, 2013),
378 outdoors (Le Breton et al., 2017) and with snow on the tags (Nummela et al., 2008). This real-world test confirms that
379 RFID adapts very well to natural outdoor areas despite periods of fog and precipitation, although minor accuracy and
380 readability degradations were noted in the presence of snow. This degradation may be due to detuning effects in the
381 vicinity of the tag and station antenna (Dobkin and Weigand, 2005) and to changes in the propagation paths (Kim et al.,
382 2012) due to snow (Larson et al., 2009) or vegetation (Kim et al., 2012). Displacement accuracy outdoors was found to
383 be ±1 cm with vegetation, precipitations, fog or frost, and in rare cases ±8 cm after snowfall. The technique is thus well
384 adapted for outdoor applications to measure displacements ranging from 1 cm to several meters.

385 The second advantage of RFID is its low cost, allowing displacements to be measured with a high spatio-temporal
386 resolution. Current prices are about 20 € per tag and 4 k per station. Moreover, the instruments were found to be robust
387 and reliable, requiring little maintenance during the experiment (zero maintenance on the tags, three reboot of the
388 station operated remotely, and one replacement of network cables degraded by animals) and providing a data
389 completeness rate of 97% over five months for most tags. Because of their low cost, a large number of tags can be
390 deployed on landslides, providing a high spatial resolution to delineate and characterize moving zones. From a
391 technical point of view, unique tag identifiers and anti-collision algorithms make simultaneous reading of hundreds of
392 densely stacked tags possible (Caizzone and Marrocco, 2011) at a rate of up to 800 tags per second (*EPC Gen2*, 2015;
393 Klair et al., 2010). This capacity results in a high spatio-temporal resolution with lightweight time series that are easy
394 to transmit and process almost in real-time. Because of these characteristics, the method could easily be incorporated in
395 an early-warning-system (Intrieri et al., 2012) and appears to be well suited for low-cost, dense monitoring applications

in high-risk environments such as landslides where devices may be destroyed.

The final advantage is the continuous development of tags to become multi-parameter sensors (Zhang et al., 2017). In this study, the tags were equipped with a temperature sensor that we used for phase calibration. Recently, other sensors have been incorporated into tags, to gather data related to tilt (Lai et al., 2018), soil moisture content (Aroca et al., 2018; Pichorim et al., 2018) and vibrations (Jayawardana et al., 2016). All these parameters could be of interest when monitoring landsides, opening new perspectives in dense sensing.

As for the limitations, the first one on landslides is currently the tag's reading range, which was limited to 60 m in this application. However, this limit (Nikitin and Rao, 2008) should rapidly evolve with the development of ultra-sensitive tags (Amato et al., 2018; Durgin, 2016) and directive tag antennas (Kim and Yeo, 2012). Therefore, a range of a few hundred meters seems to be an achievable goal in the near future.

Secondly, the measurement is limited to 1D radial displacement. Measuring a 2D or 3D translational displacement field is technically possible, but would require additional antennas and may alter measurement accuracy (Miesen et al., 2013a; Wang and Katabi, 2013). Furthermore, it is not enough to measure a purely translational displacement, as a progressive tilt of the tag's supporting stick can create a discrepancy between the ground and tag displacements that must be accounted for. This tilt could be measured in real-time by joining multiple tags (Lai et al., 2018) and corrected in the next future.

Finally, the displacements measured are affected by an ambiguity of 8.6 cm that originates from phase difference measurements. To address this problem will require first a high time resolution without missing data to avoid differential displacements exceeding this ambiguity, and second an unwrapping of the phase (Zuo et al., 2016). Unwrapping noisy or incomplete data produced by a tag could be guided by nearby high-quality data if a large number of tags are deployed, or by a previously defined rain-based model such as that presented in the application section.

6. CONCLUSIONS

RFID displacement tracking appears effective for monitoring surface deformations on a landslide, with unpreceded spatio-temporal sampling, at a significantly lower cost than GPS or ground-based radar and with an overall 1-cm accuracy within a range of 60 m including a distance-dependent error of around 150 ppm.

In the future, the technique could be enhanced by monitoring displacements in 3D, increasing the reading range, correcting for tilt of the tag support, and assessing performance in the presence of obstacles (e.g. snow, vegetation, rocks or concrete). New environmental applications could be developed by exploiting sensor tags (e.g. temperature,

tilt, soil moisture or vibrations), developing a real-time surveillance system that exploits the rapid time sampling (3-30 ms), measuring very fast displacements, and testing new outdoor applications (e.g. volcanoes, civil infrastructure, rocks, snow or vegetation). Finally, the fast pace of technological developments in RFID should lead to considerable improvements to the technique in the near future.

ACKNOWLEDGMENTS

This work was supported by Géolithe, the ANRT, the Labex OSUG@2020, the VOR program from Univ. Grenoble Alpes, and Tagsys. The authors thank Benjamin Vial for instrumentation, Antoine Guillemot for field surveys, Pascal Lacroix for insights into deformation monitoring techniques, and Hannah Taylor and Maighread Gallagher for proofreading.

REFERENCES

Akbar, M.B., Taylor, D.G., Durgin, G.D., 2015. Hybrid Inertial Microwave Reflectometry for mm-Scale Tracking in RFID Systems. IEEE Transactions on Wireless Communications 14, 6805–6814. https://doi.org/10.1109/TWC.2015.2460250

Amato, F., Torun, H.M., Durgin, G.D., 2018. RFID Backscattering in Long-Range Scenarios. IEEE Transactions on Wireless Communications 17, 2718–2725. https://doi.org/10.1109/TWC.2018.2801803

Angeli, M.-G., Pasuto, A., Silvano, S., 2000. A critical review of landslide monitoring experiences. Engineering Geology 55, 133–147. https://doi.org/10.1016/S0013-7952(99)00122-2

Arnitz, D., Muehlmann, U., Witrisal, K., 2010. UWB ranging in passive UHF RFID: proof of concept. Electronics letters 46, 1401–1402.

Aroca, R.V., Hernandes, A.C., Magalhães, D.V., Becker, M., Vaz, C.M.P., Calbo, A.G., 2018. Calibration of Passive UHF RFID Tags Using Neural Networks to Measure Soil Moisture. Journal of Sensors 2018, 1–12. https://doi.org/10.1155/2018/3436503

Arthaber, H., Faseth, T., Galler, F., 2015. Spread-Spectrum Based Ranging of Passive UHF EPC RFID Tags. IEEE Communications Letters 19, 1734–1737. https://doi.org/10.1109/LCOMM.2015.2469664

Badoux, H., Gabus, J.H., Mercanton, C.H., 1990. Les Diablerets, in Swiss Geological Atlas, sheet 1285, Swiss Fed. Off. for Water and Geol., Wabern, Switzerland.

Belle, P., Aunay, B., Bernardie, S., Grandjean, G., Ladouche, B., Mazué, R., Join, J.-L., 2014. The application of an innovative inverse model for understanding and predicting landslide movements (Salazie cirque landslides, Reunion Island). Landslides 11, 343–355. https://doi.org/10.1007/s10346-013-0393-5

Benoit, L., Briole, P., Martin, O., Thom, C., Malet, J.-P., Ulrich, P., 2015. Monitoring landslide displacements with the Geocube wireless network of low-cost GPS. Engineering Geology 195, 111–121. https://doi.org/10.1016/j.enggeo.2015.05.020

Bernardie, S., Desramaut, N., Malet, J.-P., Gourlay, M., Grandjean, G., 2015. Prediction of changes in landslide rates induced by rainfall. Landslides 12, 481–494. https://doi.org/10.1007/s10346-014-0495-8

Bièvre, G., Franz, M., Larose, E., Carrière, S., Jongmans, D., Jaboyedoff, M., 2018. Influence of environmental parameters on the seismic velocity changes in a clayey mudflow (Pont-Bourquin Landslide, Switzerland). Eng. Geol. Accepted, in revision.

Brönnimann, C.S., 2011. Effect of Groundwater on Landslide Triggering.

Caizzone, S., DiGiampaolo, E., 2015. Wireless Passive RFID Crack Width Sensor for Structural Health Monitoring. IEEE Sensors Journal 15, 6767–6774. https://doi.org/10.1109/JSEN.2015.2457455

Caizzone, S., Marrocco, G., 2011. RFID Grids: Part II —Experimentations. IEEE Transactions on Antennas and Propagation 59, 2896–2904. https://doi.org/10.1109/TAP.2011.2158974

Capparelli, G., Versace, P., 2011. FLaIR and SUSHI: two mathematical models for early warning of landslides induced by rainfall. Landslides 8, 67–79. https://doi.org/10.1007/s10346-010-0228-6

Cazeca, M.J., Mead, J., Chen, J., Nagarajan, R., 2013. Passive wireless displacement sensor based on RFID technology. Sensors and Actuators A: Physical 190, 197–202. https://doi.org/10.1016/j.sna.2012.11.007

Confidex, 2014. Survivor B Datasheet.

Corominas, J., Moya, J., Ledesma, A., Lloret, A., Gili, J.A., 2005. Prediction of ground displacements and velocities from groundwater level changes at the Vallcebre landslide (Eastern Pyrenees, Spain). Landslides 2, 83–96. https://doi.org/10.1007/s10346-005-0049-1

Das, R., 2017. RFID Forecasts, Players and Opportunities 2017-2027. IDTechEx.

Dobkin, D., Weigand, S., 2005. Environmental effects on RFID tag antennas, in: IEEE MTT-S Int. Microwave Symp. Dig. Presented at the IEEE MTT-S International Microwave Symposium Digest, Long Beach, CA, USA, pp. 135–138. https://doi.org/10.1109/MWSYM.2005.1516541

Durgin, G.D., 2016. RF thermoelectric generation for passive RFID, in: 2016 IEEE International Conference on RFID (RFID). Presented at the 2016 IEEE International Conference on RFID (RFID), pp. 1–8. https://doi.org/10.1109/RFID.2016.7488025

EM 4325 Spec. (Technical Specifications No. 420005-A01, 2.0), 2015. . EM Microelectronic - Marin SA.

EPC (tm) Radio-Frequency Identity Protocols Generation-2 UHF RFID (Standard No. 2.0.1), 2015. . EPCglobal Inc.

ETSI EN 302-208 (Standard No. 3.1.0), 2016. . ETSI.

Gage, K.S., Balsley, B.B., 1980. On the scattering and reflection mechanisms contributing to clear air radar echoes from the troposphere, stratosphere, and mesophere. Radio Sci. 15, 243–257. https://doi.org/10.1029/RS015i002p00243

Gili, J.A., Corominas, J., Rius, J., 2000. Using Global Positioning System techniques in landslide monitoring. Engineering Geology 55, 167–192. https://doi.org/10.1016/S0013-7952(99)00127-1

Griffin, J.D., Durgin, G.D., 2009. Complete Link Budgets for Backscatter-Radio and RFID Systems. IEEE Antennas and Propagation Magazine 51, 11–25. https://doi.org/10.1109/MAP.2009.5162013

Heidrich, J., Brenk, D., Essel, J., Schwarzer, S., Seemann, K., Fischer, G., Weigel, R., 2010. The Roots, Rules, and Rise of RFID. IEEE Microwave Magazine 11, 78–86. https://doi.org/10.1109/MMM.2010.936075

Intrieri, E., Gigli, G., Gracchi, T., Nocentini, M., Lombardi, L., Mugnai, F., Frodella, W., Bertolini, G., Carnevale, E., Favalli, M., Fornaciai, A., Marturià Alavedra, J., Mucchi, L., Nannipieri, L., Rodriguez-Lloveras, X., Pizziolo, M., Schina, R., Trippi, F., Casagli, N., 2018a. Application of an ultra-wide band sensor-free wireless network for ground monitoring. Engineering Geology 238, 1–14. https://doi.org/10.1016/j.enggeo.2018.02.017

Intrieri, E., Gigli, G., Mugnai, F., Fanti, R., Casagli, N., 2012. Design and implementation of a landslide early warning system. Engineering Geology 147–148, 124–136. https://doi.org/10.1016/j.enggeo.2012.07.017

Intrieri, E., Raspini, F., Fumagalli, A., Lu, P., Del Conte, S., Farina, P., Allievi, J., Ferretti, A., Casagli, N., 2018b. The Maoxian landslide as seen from space: detecting precursors of failure with Sentinel-1 data. Landslides 15, 123–133. https://doi.org/10.1007/s10346-017-0915-7

Iten, M., Puzrin, A.M., Schmid, A., 2008. Landslide monitoring using a road-embedded optical fiber sensor, in: Smart Sensor Phenomena, Technology, Networks, and Systems 2008. Presented at the Smart Sensor Phenomena, Technology, Networks, and Systems 2008, International Society for Optics and Photonics, p. 693315. https://doi.org/10.1117/12.774515

Iverson, R.M., 2000. Landslide triggering by rain infiltration. Water Resour. Res. 36, 1897–1910. https://doi.org/10.1029/2000WR900090

Jaboyedoff, M., Oppikofer, T., Abellán, A., Derron, M.-H., Loye, A., Metzger, R., Pedrazzini, A., 2012. Use of LIDAR in landslide investigations: a review. Nat Hazards 61, 5–28. https://doi.org/10.1007/s11069-010-9634-2

Jaboyedoff, M., Pedrazzini, A., Loye, A., Oppikofer, T., i Pons, M., Locat, J., 2009. Earth flow in a complex geological environment: the example of Pont Bourquin, Les Diablerets (Western Switzerland). Landslide Processes, From Geomorphologic Mapping to Dynamic Modelling 131–137.

Jayawardana, D., Kharkovsky, S., Liyanapathirana, R., Zhu, X., 2016. Measurement System With Accelerometer Integrated RFID Tag for Infrastructure Health Monitoring. IEEE Transactions on Instrumentation and Measurement 65, 1163–1171. https://doi.org/10.1109/TIM.2015.2507406

Kenney, J.D., Poole, D.R., Willden, G.C., Abbott, B.A., Morris, A.P., McGinnis, R.N., Ferrill, D.A., 2009. Precise positioning with wireless sensor nodes: Monitoring natural hazards in all terrains, in: IEEE Int. Conf. Systems, Man and Cybernetics. Presented at the IEEE International Conference on Systems, Man and Cybernetics, San Antonio, TX, USA, pp. 722–727. https://doi.org/10.1109/ICSMC.2009.5346714

Kim, D., Yeo, J., 2012. Dual-Band Long-Range Passive RFID Tag Antenna Using an AMC Ground Plane. IEEE Transactions on Antennas and Propagation 60, 2620–2626. https://doi.org/10.1109/TAP.2012.2194638

Kim, Y., Jackson, T., Bindlish, R., Lee, H., Hong, S., 2012. Radar Vegetation Index for Estimating the Vegetation Water Content of Rice and Soybean. IEEE Geoscience and Remote Sensing Letters 9, 564–568. https://doi.org/10.1109/LGRS.2011.2174772

Klair, D.K., Kwan-Wu Chin, Raad, R., 2010. A Survey and Tutorial of RFID Anti-Collision Protocols. IEEE Communications Surveys & Tutorials 12, 400–421. https://doi.org/10.1109/SURV.2010.031810.00037

Lacroix, P., Bièvre, G., Pathier, E., Kniess, U., Jongmans, D., 2018. Use of Sentinel-2 images for the detection of precursory motions before landslide failures. Remote Sensing of Environment. https://doi.org/10.1016/j.rse.2018.03.042

Lai, X., Cai, Z., Xie, Z., Zhu, H., 2018. A Novel Displacement and Tilt Detection Method Using Passive UHF RFID Technology. Sensors 18, 1644. https://doi.org/10.3390/s18051644

Lamarre, H., MacVicar, B., Roy, A.G., 2005. Using Passive Integrated Transponder (PIT) Tags to Investigate Sediment Transport in Gravel-Bed Rivers. Journal of Sedimentary Research 75, 736–741. https://doi.org/10.2110/jsr.2005.059

Larson, K.M., Gutmann, E.D., Zavorotny, V.U., Braun, J.J., Williams, M.W., Nievinski, F.G., 2009. Can we measure snow depth with GPS receivers? Geophys. Res. Lett. 36, L17502. https://doi.org/10.1029/2009GL039430

Le Breton, M., Baillet, L., Larose, E., Rey, E., Benech, P., Jongmans, D., Guyoton, F., 2017. Outdoor UHF RFID: Phase Stabilization for Real-World Applications. IEEE Journal of Radio Frequency Identification 1, 279–290. https://doi.org/10.1109/JRFID.2017.2786745

Lucianaz, C., Greco, G., Bertoldo, S., Allegretti, M., 2015. Real time outdoor localization of buried RFID tags through statistical methods, in: Int. Conf. on Electromagnetics in Advanced Applications. Presented at the International Conference on Electromagnetics in Advanced Applications (ICEAA), pp. 1152–1154. https://doi.org/10.1109/ICEAA.2015.7297299

M. H. Nichols, 2004. A Radio Frequency Identification System for Monitoring Coarse Sediment Particle Displacement. Applied Engineering in Agriculture 20, 783–787. https://doi.org/10.13031/2013.17727

Miesen, R., Ebelt, R., Kirsch, F., Schäfer, T., Li, G., Wang, H., Vossiek, M., 2011. Where is the Tag? IEEE Microwave Magazine 12, S49–S63. https://doi.org/10.1109/MMM.2011.942730

Miesen, R., Kirsch, F., Vossiek, M., 2013a. UHF RFID Localization Based on Synthetic Apertures. IEEE Transactions on Automation Science and Engineering 10, 807–815. https://doi.org/10.1109/TASE.2012.2224656

Miesen, R., Parr, A., Schleu, J., Vossiek, M., 2013b. 360° carrier phase measurement for UHF RFID local positioning, in: 2013 IEEE International Conference on RFID-Technologies and Applications (RFID-TA). Presented at the 2013 IEEE International Conference on RFID-Technologies and Applications (RFID-TA), pp. 1–6. https://doi.org/10.1109/RFID-TA.2013.6694499

Milillo, P., Fielding, E.J., Shulz, W.H., Delbridge, B., Burgmann, R., 2014. COSMO-SkyMed Spotlight Interferometry Over Rural Areas: The Slumgullion Landslide in Colorado, USA. IEEE Journal of Selected Topics in Applied Earth Observations and Remote Sensing 7, 2919–2926. https://doi.org/10.1109/JSTARS.2014.2345664

Monserrat, O., Crosetto, M., Luzi, G., 2014. A review of ground-based SAR interferometry for deformation measurement. ISPRS Journal of Photogrammetry and Remote Sensing 93, 40–48. https://doi.org/10.1016/j.isprsjprs.2014.04.001

Ngai, E.W.T., Moon, K.K.L., Riggins, F.J., Yi, C.Y., 2008. RFID research: An academic literature review (1995–2005) and future research directions. International Journal of Production Economics, Special Section on RFID: Technology, Applications, and Impact on Business Operations 112, 510–520. https://doi.org/10.1016/j.ijpe.2007.05.004

Ni, L.M., Liu, Y., Lau, Y.C., Patil, A.P., 2003. LANDMARC: indoor location sensing using active RFID, in: Proceedings of the First IEEE International Conference on Pervasive Computing and Communications, 2003. (PerCom 2003). Presented at the Proceedings of the First IEEE International Conference on Pervasive Computing and Communications, 2003. (PerCom 2003), pp. 407–415. https://doi.org/10.1109/PERCOM.2003.1192765

Nikitin, P.V., Martinez, R., Ramamurthy, S., Leland, H., Spiess, G., Rao, K.V.S., 2010. Phase based spatial identification of UHF RFID tags, in: IEEE Int. Conf. RFID. Presented at the IEEE International Conference on RFID, IEEE, Orlando, FL, USA, pp. 102–109.

Nikitin, P.V., Rao, K.V.S., 2008. Antennas and propagation in UHF RFID systems. Presented at the IEEE International Conference on RFID, Las Vegas, USA, p. 23.

Nummela, J., Ukkonen, L., Sydänheimo, L., 2008. Passive UHF RFID tags in arctic environment. International Journal of Communications 2, 135–142.

Pedregosa, F., Varoquaux, G., Gramfort, A., Michel, V., Thirion, B., Grisel, O., Blondel, M., Prettenhofer, P., Weiss,

R., Dubourg, V., Vanderplas, J., Passos, A., Cournapeau, D., Brucher, M., Perrot, M., Duchesnay, É., 2011. Scikit-learn: Machine Learning in Python. Journal of Machine Learning Research.

Pichorim, S., Gomes, N., Batchelor, J., 2018. Two Solutions of Soil Moisture Sensing with RFID for Landslide Monitoring. Sensors 18, 452. https://doi.org/10.3390/s18020452

Scherhäufl, M., Pichler, M., Stelzer, A., 2015. UHF RFID Localization Based on Phase Evaluation of Passive Tag Arrays. IEEE Transactions on Instrumentation and Measurement 64, 913–922. https://doi.org/10.1109/TIM.2014.2363578

Tibshirani, R., 1996. Regression Shrinkage and Selection via the Lasso. Journal of the Royal Statistical Society. Series B (Methodological) 58, 267–288.

Travelletti, J., Delacourt, C., Allemand, P., Malet, J.-P., Schmittbuhl, J., Toussaint, R., Bastard, M., 2012. Correlation of multi-temporal ground-based optical images for landslide monitoring: Application, potential and limitations. ISPRS Journal of Photogrammetry and Remote Sensing 70, 39–55. https://doi.org/10.1016/j.isprsjprs.2012.03.007

Tzeng, S.-F., Chen, W.-H., Pai, F.-Y., 2008. Evaluating the business value of RFID: Evidence from five case studies. International Journal of Production Economics 112, 601–613. https://doi.org/10.1016/j.ijpe.2007.05.009

Vossiek, M., Gulden, P., 2008. The Switched Injection-Locked Oscillator: A Novel Versatile Concept for Wireless Transponder and Localization Systems. IEEE Transactions on Microwave Theory and Techniques 56, 859–866. https://doi.org/10.1109/TMTT.2008.918158

Wang, J., Katabi, D., 2013. Dude, Where's My Card?: RFID Positioning That Works with Multipath and Non-line of Sight, in: Proceedings of the ACM SIGCOMM 2013 Conference on SIGCOMM, SIGCOMM '13. ACM, New York, NY, USA, pp. 51–62. https://doi.org/10.1145/2486001.2486029

Wang, Z., Ye, N., Malekian, R., Xiao, F., Wang, R., 2016. TrackT: Accurate tracking of RFID tags with mm-level accuracy using first-order taylor series approximation. Ad Hoc Networks 53, 132–144. https://doi.org/10.1016/j.adhoc.2016.09.026

Zhang, J., Tian, G.Y., Marindra, A.M.J., Sunny, A.I., Zhao, A.B., 2017. A Review of Passive RFID Tag Antenna-Based Sensors and Systems for Structural Health Monitoring Applications. Sensors 17, 265. https://doi.org/10.3390/s17020265

Zhou, C., Griffin, J.D., 2012. Accurate phase-based ranging measurements for backscatter RFID tags. IEEE Antennas and Wireless Propagation Letters 11, 152–155.

Zuo, C., Huang, L., Zhang, M., Chen, Q., Asundi, A., 2016. Temporal phase unwrapping algorithms for fringe projection profilometry: A comparative review. Optics and Lasers in Engineering 85, 84–103. https://doi.org/10.1016/j.optlaseng.2016.04.022